Solar Energy
and Sustainable Development
Refereed, biannual scientific journal issued by
The Libyan Center for Solar Energy Research and Studies

Exploring the Optoelectronic and Photocatalytic Properties of $SrMg_2FeH_8$ for Advanced Energy Applications

Hamza Errahoui*[1], Mohamed Karouchi[1], Abdelkebir Ejjabli[1], Abdelmounaim Laassouli[1] Aymane EL HAJI [1], Youssef Lachtioui[1], and Omar Bajjou[1].

[1]Laboratory of Engineering in Chemistry and Physics of Matter Faculty of Sciences and Technics, Sultan Moulay Slimane University, BP 523, 23000, Beni Mellal, Morocco.

E-*mail:* [1] hamzaa.errahoui@gmail.com

ARTICLE INFO.

Article history:
Received 21 June 2025
Received in revised form
06 November 2025
Accepted 05 December 2025

Available online 25 March 2026

KEYWORDS

Hydride compounds, Optoelectronic properties, Photocatalysis, Band gap, Optical absorption, Hydrogen production

ABSTRACT

$SrMg_2FeH_8$ is a type of hydride compound that shows a lot of promise for use in optoelectronics and photocatalysis. I've analyzed its electronics structure to understand its function better. An analysis of its total electronic states shows that it behaves like a semiconductor with a moderate bandgap of 2.251 eV. For the purposes of photocatalysis, the bandgap is advantageous as it means that the material can absorb visible light quite readily. The examination related to materials optical properties - in terms of its refractive index and light absorption - confirms strong absorption to light in the visible and ultraviolet ranges. All of these characteristics make it a very worthwhile specimen for use in optoelectronic devices.

The photocatalytic capacity of $SrMg_2FeH_8$ has been thoroughly studied with interest in its capacity to promote both oxidation and reduction reactions. The valence band edge located at 2.61 eV referenced to the normal hydrogen electrode would suggest it should be suitable to promote water oxidation processes. The conduction band edge was located at 0.36 eV, again referenced to the normal hydrogen electrode and while this described hydrogen evolution, it would seem kinetic limitations will require the use of co-catalysts in order to utilize hydrogen evolution efficiently.

The strong optical absorption, combined with its electronics and photocatalytic properties, provides positive results for potential applications in hydrogen production, pollutant degradation and energy conversion technologies.

*Corresponding author.

DOI: https://doi.org/10.51646/jsesd.v14i2.630

استكشاف الخصائص البصرية والإلكترونية والضوئية التحفيزية لمركب $SrMg_2FeH_8$، لتطبيقات الطاقة المتقدمة

حمزة الرحوي، محمد كروشي، عبد الكبير الجبلي، عبد المنعم العسولي ، أيمن الحاجي، يوسف لشتيوي ، عمر باجو

ملخص: يُعد مركب SrMg2FeH8 نوعًا من المركبات الهيدريدية التي تظهر إمكانات كبيرة للاستخدام في الإلكترونيات البصرية والتحفيز الضوئي. تم تحليل البنية الإلكترونية له لفهم وظائفه بشكل أفضل. تُظهر دراسة الحالات الإلكترونية الكلية للمركب أنه يتصرف كمواد شبه موصلة مع فجوة نطاق معتدلة تبلغ 2.251 إلكترون فولت، فيما يخص التحفيز الضوئي، تُعد فجوة النطاق مناسبة لأنها تسمح للمادة بامتصاص الضوء المرئي بسهولة كبيرة.

كما أكدت الدراسة المتعلقة بالخصائص البصرية للمادة من حيث معامل الانكسار وامتصاص الضوء وجود امتصاص قوي للضوء في نطاقي الضوء المرئي وفوق البنفسجي. كل هذه الخصائص تجعل المركب نموذجًا جديرًا بالاستخدام في الأجهزة البصرية الإلكترونية. تمت دراسة القدرة التحفيزية الضوئية لمركب SrMg2FeH8 بشكل شامل، مع التركيز على قدرته على ت تعزيز كل من تفاعلات الأكسدة والاختزال. يقع حافة نطاق التكافؤ عند 2.61 إلكترون فولت بالنسبة إلى قطب الهيدروجين ة القياسي، مما يشير إلى أنه مناسب لتعزيز عمليات أكسدة الماء. أما حافة نطاق التوصيل، فتم تحديدها عند 0.36 إلكترون فول بالنسبة إلى نفس المرجع، وتشير إلى إمكانية إنتاج الهيدروجين، إلا أن القيود الحركية قد تتطلب استخدام محفزات مشترك لتحقيق تطور الهيدروجين بكفاءة.

يمثل الامتصاص البصري القوي، جنبًا إلى جنب مع الخصائص الإلكترونية والتحفيزية الضوئية، نتائج إيجابية للتطبيقات المحتملة في إنتاج الهيدروجين، وتحليل الملوثات، وتقنيات تحويل الطاقة.

الكلمات المفتاحية: المركبات الهيدريدية، الخصائص البصرية والإلكترونية، التحفيز الضوئي، فجوة النطاق، امتصاص الضوء، إنتاج الهيدروجين.

1. INTRODUCTION

Recent research into complex hydrides has generated substantial interest because of potentially useful applications in a wide domain of technologies such as energy storage, optoelectronic devices, and photocatalysis[1–3]. Complex hydrides consist of hydrogen atoms bonded to metallic or metalloid atoms which often structure into complex crystalline forms defined by specific bonding interactions[4,5]. This family of materials becomes significant due to the overall light-weight properties while also being tunable in physical and chemical properties. Transition metal-based hydrides among them have been specifically interesting due to being particularly versatile and have shown that they can demonstrate significant properties in areas of electronics and optics[6,7]. $SrMg_2FeH_8$ in particular with its unique structural, electronic, and compositional properties is being chosen as a material that has a great potential for investigations.

Hydrides of transition metals, especially hydrides of iron (Fe), display interesting optoelectronic properties as the transition metal has partially filled d orbitals[3,7]. These optoelectronic properties can enhance light absorption, charge transfer processes, and catalytic activity which are benefiting for next generation energy systems. The addition of alkaline-earth metals, in particular strontium (Sr) and magnesium (Mg) add other degrees of freedom to modify the electronic band structural and optical response of the hydride lattice. The Sr component will serve to impart strong ionic bonding to increase structural stability, whereas the Mg will provide the structure sufficient light-weight and strong framework which imparts function[8–10]. Collectively, these combinations imply that $SrMg_2FeH_8$ should be an exciting material for new functional applications. Previous investigations on related Fe-based complex hydrides, such as Mg_2FeH_8–$LiBH_4$ and Mg_2FeH_8–$LiNH_2$ composites, have shown promising hydrogen storage capacities [11–13]. These studies demonstrate the scientific relevance of Fe-

containing hydrides in energy-related applications. Having said that, complex hydrides offer additional interesting properties as well; in addition to the structural and electronic flexibility, they are environmentally friendly and have the capacity for hydrogen storage or solar-powered catalysis[3]. Recent progress in hydrogen storage materials has been extensively reviewed, with particular attention to complex and lightweight hydrides due to their high hydrogen content and tunable electronic properties [14,15]. These advances provide important insights for designing new hydrides with enhanced structural stability and hydrogen storage performance. The compound $SrMg_2FeH_8$ was first synthesized and experimentally characterized by Huang et al. in 1992 using X-ray and neutron diffraction techniques, which revealed a complex hydride structure containing octahedral $[FeH_6]^{4-}$ units embedded within a Sr–Mg matrix [16,17]. $SrMg_2FeH_8$ is particularly exciting as it is a hydrogen-rich structure that can be advantageous for hydrogen storage technologies. In addition to the ability to entrap significant amounts of hydrogen, this structure is also attractive for applications in hydrogen-based energy systems and contributes to a clean energy economy[18]. This hydrogen-rich structural property may be useful used for water splitting or other renewable energy applications[19,20]. By analyzing its optical absorption, electronic transitions, and density of states (DOS), the data gives valuable understanding of its performance with respect to numerous conditions and assists in the development of specific customized solutions relative to the desired technological goals.

This study examines the optoelectronic and photocatalytic properties of $SrMg_2FeH_8$ using theoretical and computational techniques. Specifically, the study looks at light absorption, the real and imaginary parts of the dielectric function of the material, and also conductivity, loss function, and refractive index. By looking at these properties, the study will showcase its possible use as a photocatalyst, optoelectronic device material, and a medium for hydrogen storage, which will provide a fundamental insight into transition metal hydrides and useful knowledge in the context of applied physics and engineering.

2. MATERIALS AND METHODS

This work implemented density functional theory (DFT) calculations to study the optoelectronic and photocatalytic properties of $SrMg_2FeH_8$, specifically through the use of the scientific simulation software in $CASTEP$[21–23]. Within this work, the meta-generalized gradient approximation ($m-GGA$) for the exchange-correlation functional was utilized owing to the complex electronic interactions present in complex hydrides and increased accuracy in theoretical predictions of electronic structure made well-established from literature[24–26]. Within the methodology, a plane wave basis set with a kinetic energy cutoff of $500\ eV$ was employed to achieve a balance between numerical convergence and computational efficiency for accurate results. Brillouin zone integration was completed using a Monkhorst-Pack $3 \times 3 \times 2$ k-point mesh identifying with the crystal symmetry of $SrMg_2FeH_8$ and provided the resolution needed for meaningful electronic structure analysis[27].

The careful optimization of all contributing computational parameters was a key contributor to the accurate representation of the band structure, density of states, and optical absorption properties.

The compound $SrMg_2FeH_8$ possesses a trigonal crystal structure in the $P\bar{3}m1$ space group. The strontium (Sr^{2+}) atom is coordinated by twelve hydride (H-) anion atoms, forming cuboctahedral SrH_{12} units. The cuboctahedral units are connected through edge-sharing with six additional SrH_{12} cuboctahedra, and through face-sharing with two FeH_6 octahedra. The bond length between $Sr-L$ and H is uniform at 2.64 Å. Magnesium (Mg^{2+}) is coordinated to a total of ten hydride anions, and the range for bond distances to hydrides ranged from 1.90 Å and 2.24 Å. Iron (Fe^{2+}) is coordinated to six hydride anions with distorted geometries to form

an FeH6 octahedron (which also face shares with two SrH_{12} cuboctahedra). The bond length between Fe and H exists as a record of 1.56 Å. There are two areas of hydride in contrast to other hydrogen-containing phases outlined in this thesis, where each hydride in site one is coordinated to one Sr^{2+}, three Mg^{2+}, and one Fe^{2+} in a distorted coordination sphere, and the hydrides in site two are coordinated with three Sr^{2+} and one Mg^{2+} in a distorted geometry. The optimized lattice parameters obtained from DFT (a = 4.47 Å, c = 6.52 Å) show excellent agreement with the experimental neutron diffraction data reported by Huang et al (table 1) [16]. (a = 4.5072 Å, c = 6.5663 Å), confirming the reliability and accuracy of the present structural optimization. The atomic coordinates of Sr, Mg, Fe, and H also display close correspondence, demonstrating the robustness of the computational model. The fully relaxed crystal structure of $SrMg_2FeH_8$ is illustrated in Figure 1.

Table 1. Comparison Between Experimental and DFT-Optimized Parameters

Parameter	Experimental [16]	This Work (DFT)
Space group	P-3m1 (No. 164)	P-3m1 (No. 164)
a (Å)	4.5072	4.47
c (Å)	6.5663	6.52
Volume (Å³)	—	112.75
Fe (1a)	(0, 0, 0)	(0, 0, 0)
Sr (1b)	(0, 0, 0.5)	(0, 0, 0.5)
Mg (2d)	(0.3333, 0.6667, 0.1223)	(0.667, 0.333, 0.8771)
H1 (6i)	(0.1617, −x, 0.8557)	(0.3218, 0.1609, 0.1435)
H2 (2d)	(0.3333, 0.6667, 0.4147)	(0.667, 0.333, 0.5857)

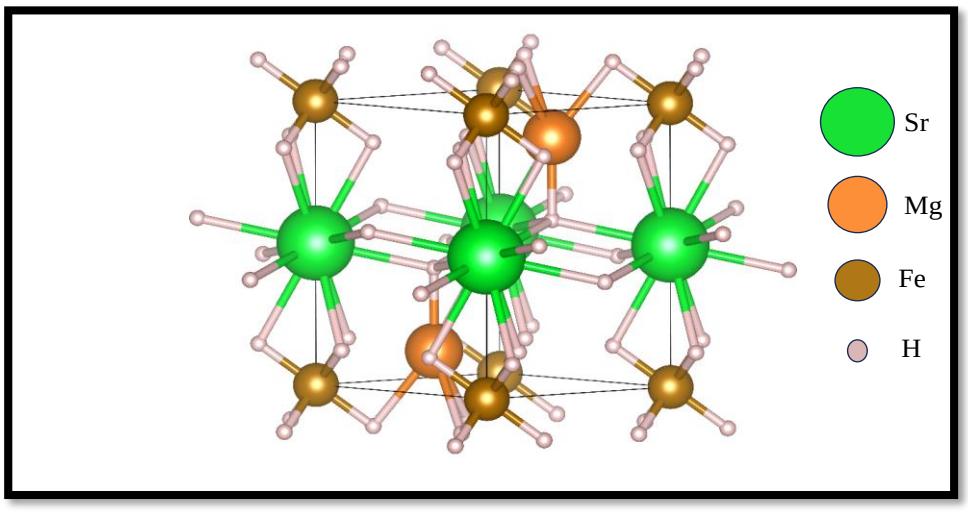

Figure 1. Crystal structure of $SrMg_2FeH_8$.

3. RESULTS AND DISCUSSIONS

3.1. Electronic Properties (Band Structure and Density of States)

Band structure of a material describes the correlation between the energy levels of electrons and their momentum in a crystal-like solid. This concept is fundamental under solid-state physics and can provide meaningful insight into a material's electronic properties, including conductivity, optical absorption, and carrier transport [28,29]. Understanding the

band structure is crucial for predicting the performance of materials in applications like optoelectronics, photocatalysis, and hydrogen storage[3,30]. $SrMg_2FeH_8$'s band structure shown in Figure 2 presents an indirect band gap of 2.251 eV, with the valence band maximum (VBM) and conduction band minimum (CBM) located at different k-points in the $Brillouin$ zone. This indirect band gap requires phonon involvement for electron excitation, which is worse for direct optical efficiencies, but preferable for thermal stability and carrier lifetime. The band gap value, falling in the visible light region suggests $SrMg_2FeH_8$ can capture visible light from the sun, providing a desirable photocatalyst property. Thus, $SrMg_2FeH_8$ with visible light-absorption capability as well as indirect band gap may be ideal in applications such as water splitting, degrading different pollutants, evolving hydrogen, or storing hydrogen.[31–33].

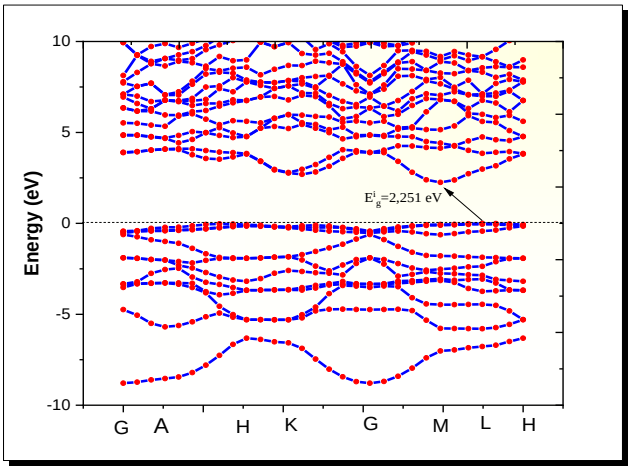

Figure 2. Band structures of $SrMg_2FeH_8$.

The total and projected density of states (DOS and $PDOS$) provide meaningful information about the electronic states of $SrMg_2FeH_8$, illuminating its semiconducting nature and emphasizing its potential for use in more advanced technologies[34]. As shown in the DOS plot (figure 3.a), there is a calculated indirect band gap of approximately 2.251 eV placing the material in the visible light range, indicating efficient light absorption as critical in optoelectronic and photocatalytic properties. The DOS plot shows a high density of states in the valence band going from -10 eV up to the $Fermi$ level (0 eV), indicating very strong electronic interactions, while the conduction band starts in states above the $Fermi$ energy level, indicating the materials potential for electron excitation and transport[35,36]. The $PDOS$ analysis (figure 3.b) further divides these classes of electronic states into their constituent contributions, and it is evident that hydrogen (H) acts primarily through the s orbitals with a dominant contribution to the valence band, demonstrating a strong bond with the metallic elements. Iron (Fe) is indicative of the importance of its d states, prevalent near the Fermi level and prevalent in both the valence and conduction bands, facilitating the importance of electronic transitions for photocatalysis. Magnesium (Mg) contributes predominantly to the electronic structure through its s and p orbitals aspects, stabilizing the structure and allowing secondary contributions as an electronic component, strontium contributes to the optical absorption and conduction properties of the material through its d orbitals, which extend into the conduction band. The interaction between the Fe, H, Mg, and Sr orbitals are not only

responsible for the electronic and optical properties of $SrMg_2FeH_8$, but the multifaceted interaction provides a platform and continuum for possible applications as a multifunctional material. Overall, the insights from both the DOS and $PDOS$ contribute to an optimistic outlook towards $SrMg_2FeH_8$ in energy-related technologies due to the band gap, strong orbital interactivity, and beneficial carrier dynamics.[37,38].

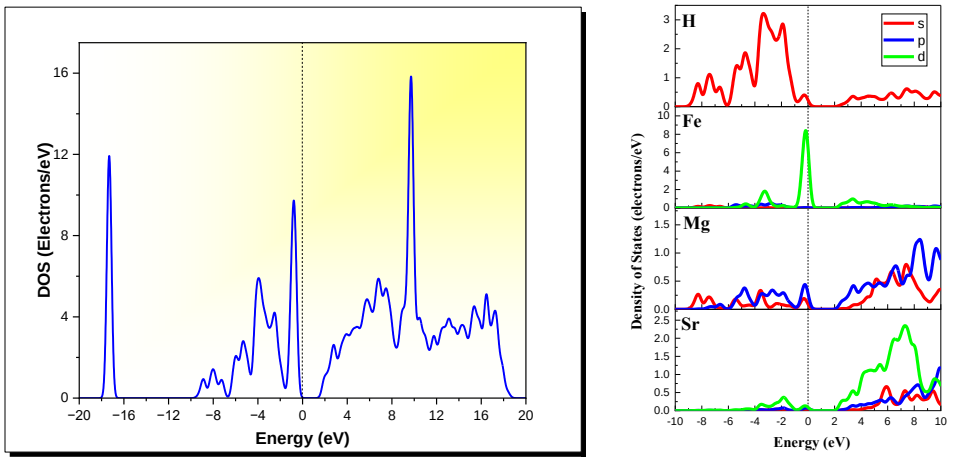

(a) (b)

Figure 3. a) DOS; b) PDOS of $SrMg_2FeH_8$.

3.2 Optical Properties.

3.2.1 Dielectric Function, refractive index and extinction coefficient.

The optical response of a material can be obtained from how different optical parameters change as a function of the energy of the incoming photons ($E = h\nu$) or from the frequency of incoming radiation. An important component in discerning this behavior is the complex dielectric function $\varepsilon(\omega)$, which is a function of the frequency of incoming radiation. The dielectric function provides valuable information about the interaction of the material with electromagnetic waves and is fundamental to understanding many optical phenomena. The mathematical expression for $\varepsilon(\omega)$ is shown below.[39,40]:

$$\varepsilon(\omega) = \varepsilon_1(\omega) + i\,\varepsilon_2(\omega) \qquad (1)$$

The electronic band structure of a material significantly influences its dielectric response, as changes in the electronic states will alter the way that the material interacts with light. Indeed, the dielectric function's imaginary part $\varepsilon_2(\omega)$, directly related to the optical absorption properties, can be determined from the following equation [41,42]:

$$\varepsilon_2(\omega) = \left(\frac{\hbar^2 e^2}{\pi m^2 \omega^2}\right) \sum_{c,v} \int d^3k \langle c_k|\, p^{\alpha} |v_k\rangle \langle v_k|\, p^{\beta} |c_k\rangle x \delta\left(\varepsilon_{c_k} - \varepsilon_{v_k} - \omega\right) \qquad (2)$$

The momentum matrix element, p, describes the transition probability between electronic states α and β at a crystal momentum k. In this context, c_k and v_k are the conduction and

valence band states, respectively. For the two states, k is the crystal wave vector. The real part of the dielectric function, $\varepsilon_1(\omega)$, can be obtained from the imaginary part, $\varepsilon_2(\omega)$ via the Kramers-Kronig Transformation, shown in the equation below[43]:

$$\varepsilon_1(\omega) = 1 + \frac{2}{\pi} \mathrm{p} \int_0^{\infty} \frac{\omega' \varepsilon_2(\omega')}{(\omega')^2 - \omega^2} \mathrm{d}\omega' \quad (3)$$

where p denotes the integral's primary value.

The zero-frequency limit of the real part of the dielectric function, denoted as $\varepsilon_1(0)$, is a key parameter that reflects the purely electronic contribution to the static dielectric response. Its mathematical formulation is given as follows [44]:

$$\varepsilon_1(0) \approx 1 + \left(\frac{h\omega}{E_g}\right) \quad (4)$$

The optical properties of $SrMg_2FeH_8$ were analyzed through the real part $\varepsilon_1(\omega)$ and imaginary part $\varepsilon_2(\omega)$ components of the dielectric function (Figure 4). The real part, $\varepsilon_1(\omega)$ describes the material's ability to store electrical energy and its dispersion behavior as a function of incident photon energy[45]. At zero energy, $\varepsilon_1(0)$ has a value of 4.2, indicating significant polarizability at low frequencies, corresponding to the static dielectric constant. A prominent peak at 4.95 eV with a maximum value of 6.89 indicates strong electronic polarizability due to interband transitions, involving contributions from Fe d-orbitals and H s-orbitals. At energies greater than approximately 10 eV, $\varepsilon_1(\omega)$ is negative; this indicates metallic-like behavior and that reflectivity or absorption are defining the regions of interest. In addition, the imaginary part $\varepsilon_2(\omega)$, informs users on aspects of the optical absorption characteristics and on the electronic transitions. Optical absorption starts at approximately 2.2 eV which corresponds to the indirect bandgap thus confirming that the material is capable of absorbing photons in the visible region of the spectrum.

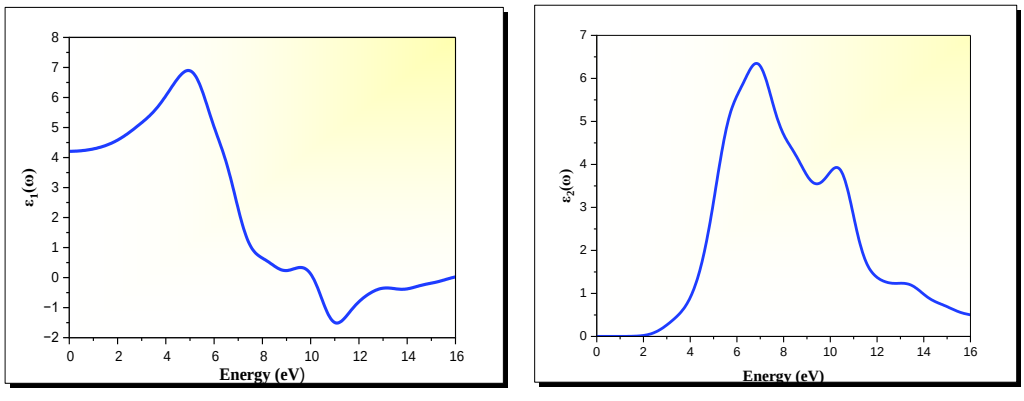

(a) (b)

Figure 4. a) Real part of dielectric function, b) Imaginary part of dielectric function of $SrMg_2FeH_8$.

The peak value of 6.34 occurs at 6.83 eV and is indicative of strong interband transitions involving Fe d-orbitals close to the Fermi level and contributions from H s-orbitals. Other

peaks at higher energies (e.g. 8 eV) are associated with some transitions involving the Mg and Sr orbitals that are in the conduction band. The decrease would suggest that there are fewer electronic states available for transitions beyond 8 eV [46].

The findings describe the robust optical activity exhibited by $SrMg_2FeH_8$ in the visible-to-near-UV region, and this evidence, in addition to electronic bandgap and structural parameters, supports $SrMg_2FeH_8$ in potential applications, such as: photocatalysis, optoelectronic devices, and renewable energy. The complementary electronic and optical properties add credibility to $SrMg_2FeH_8$ as a multifunctional material for advanced technological applications.

To gain a complete comprehension of the optical to optical properties of $SrMg_2FeH_8$ (figure 5) we investigated the refractive index $n(\omega)$ and extinction coefficient $k(\omega)$ compared to the components of the dielectric function, which relate to each other in a fundamental way to the real $\varepsilon_1(\omega)$ and imaginary $\varepsilon_2(\omega)$parts of the dielectric function in the following manner[9,13]:

$$n(\omega) = \frac{1}{\sqrt{2}}\left[\sqrt{\varepsilon_1^2(\omega) + \varepsilon_2^2(\omega)} + \varepsilon_1(\omega)\right]^{\frac{1}{2}} \quad (5)$$

$$k(\omega) = \frac{1}{\sqrt{2}}\left[\sqrt{\varepsilon_1^2(\omega) + \varepsilon_2^2(\omega)} - \varepsilon_1(\omega)\right]^{\frac{1}{2}} \quad (6)$$

The refractive index $n(\omega)$ which described how light propagates, is tied to the imaginary and real parts of the dielectric function. At photon energy of zero the static refractive index $n(0)$ is 2.05 corresponding to the static dielectric constant $\varepsilon 1(0)$ ($n(0) = \sqrt{\varepsilon_1(0)}$), which primarily describes polarizability at low frequencies[9,39].

This demonstrates the material's ability to store and slow down light at low energy levels. As photon energy increases, $n(\omega)$ rises, reaching a peak value of 2.69 at 5.101 eV, associated with strong dispersion due to electronic polarizability and interband transitions.

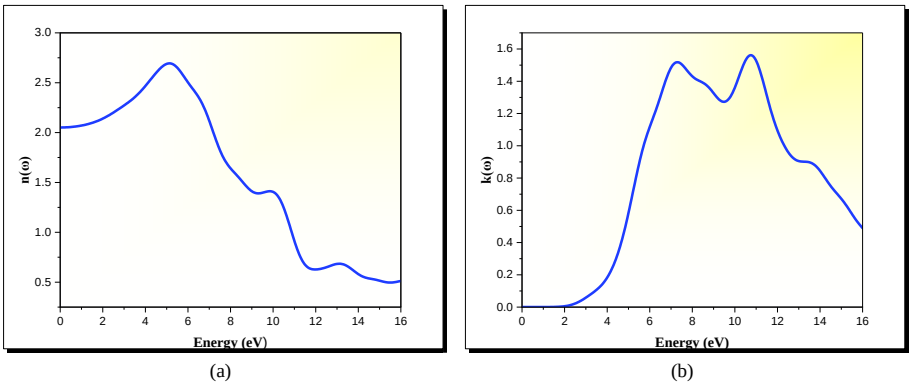

(a) (b)

Figure 5. a) Refractive index; b) Extinction coefficient of $SrMg_2FeH_8$.

These transitions are attributed to electronic excitations involving Fe d-orbitals and H s-orbitals. The extinction coefficient $k(\omega)$, which characterizes the material's light absorption, is directly influenced by $\varepsilon_1(\omega)$ and $\varepsilon_2(\omega)$. It approaches zero up to 2.18 eV, consistent with the bandgap of $SrMg_2FeH_8$, and it must be transparent in this energy range. This is similar to the imaginary part of the dielectric function $\varepsilon_2(\omega)$, which starts increasing past the bandgap.

Beyond this bandgap, at higher energies, k(ω) has two large peaks. The peaks take values of 1.51 at 7.37 eV and 1.55 at 10.83 eV. They correspond to strong absorption because of interband electronic transitions, particularly Fe d-orbitals and other orbital contributions from Mg and Sr atoms.

The connection of $\varepsilon_1(\omega)$, $\varepsilon_2(\omega)$, $n(\omega)$, and $k(\omega)$ reveals the dual optical nature of SrMg2FeH8. It acts as a transparent material at low energies while acting as an absorbing material through the visible and UV range, characterizing it as a good material for optoelectronic and photocatalytic uses. The connectivity is an advanced highlight of the optical characteristics of the material for use in energy conditions and equipment including optical devices.

3.2.2 Absorption Coefficient and Loss function.

The optical absorption coefficient $\alpha(\omega)$, and the energy loss function $L(\omega)$, of $SrMg_2FeH_8$ (Figure 6) were analyzed as the photonic and dissipative properties of the material, respectively, by determining the absorption coefficient $\alpha(\omega)$, which represents the ability of the material to absorb photons, using the relation[9,39]:

$$\alpha(\omega) = \sqrt{2}\omega[\sqrt{\varepsilon_1^2(\omega) + \varepsilon_2^2(\omega)} - \varepsilon_1(\omega)]^{\frac{1}{2}} \quad (7)$$

This parameter takes the value of zero, and remains negligible until 2.23 eV, which corresponds to the transparency of the material at the low-energy end. As photon energy increases $\alpha(\omega)$ increases rapidly, reaches a maximum value of 2.7×10^5 cm^{-1} at 10.98 eV. This peak shows that there are strong electronic transitions that will efficiently use the high-energy photons that demonstrate $SrMg_2FeH_8$ are good absorbers for optoelectronic and photocatalytic applications. The energy loss function $L(\omega)$, demonstrating the energy losses of fast electrons traveling through the material, is defined as[9]:

$$L(\omega) = \frac{\varepsilon_2(\omega)}{\varepsilon_1^2(\omega)+\varepsilon_2^2(\omega)} \quad (8)$$

The function has a value of zero, a low value from zero to 2 eV, and a low overall response until 4 eV. Beyond those values, $L(\omega)$ raises significantly, peaking at 16.98 eV with a value of 2.18.

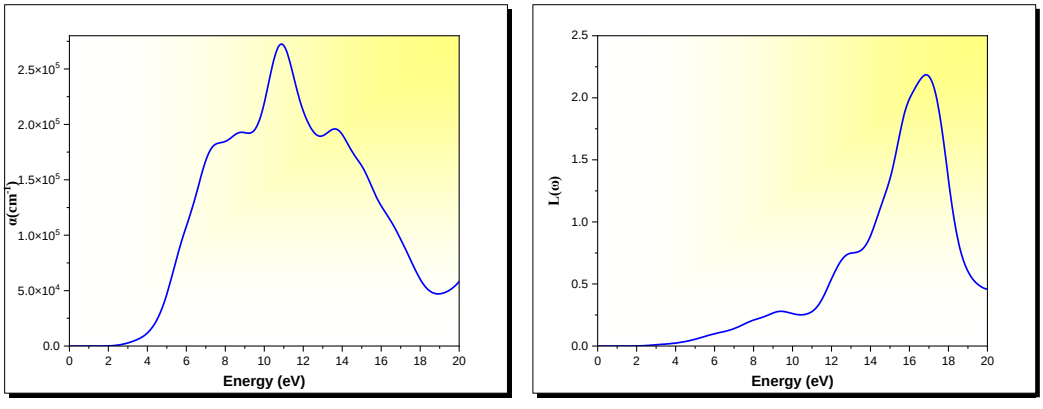

(a) (b)

Figure 6. a) Absorption; b) loss function of $SrMg_2FeH_8$.

This peak represents the plasmonic resonances which are collective oscillations of free electrons, including their interactions with the lattice of the material studied. The analysis of $\alpha(\omega)$ and $L(\omega)$, provide a view of the dual optical system that is also displayed within $SrMg_2FeH_8$. The material demonstrates transparency at low energies, strong photon absorption at higher energies, and pronounced plasmonic activity, establishing its relevance for photonic, plasmonic, and energy-related applications.

3.2.3 Reflectivity and conductivity

The reflectivity $R(\omega)$ of $SrMg_2FeH_8$ (Figure 7) was analyzed to understand its optical response to incident electromagnetic waves. Reflectivity, defined as the ratio of the reflected light intensity to the incident light intensity, measures how effectively a material reflects light at different photon energies. The reflectivity is calculated using the equation[9,39]:

$$R(\omega) = \left[\frac{\sqrt{\varepsilon_1(\omega)+i\,\varepsilon_2(\omega)}-1}{\sqrt{\varepsilon_1(\omega)+i\,\varepsilon_2(\omega)}+1}\right]^2 \quad (9)$$

In the low-energy region (0 eV to 3 eV), the reflectivity varies between 0.11 and 0.14, indicating weak reflectance, characteristic of low-energy photon interactions. Beyond 3 eV, the reflectivity increases steadily and reaches its peak value of 0.40 at 11.32 eV. This peak corresponds to strong interaction between incident photons and the electronic structure of the material, resulting in maximum reflectance. The trend of $R(\omega)$ across the energy spectrum highlights the material's selective reflectance properties, with significant reflectance at higher photon energies. This feature suggests potential applications in optoelectronic devices, where control over reflectivity is crucial for optimizing performance.

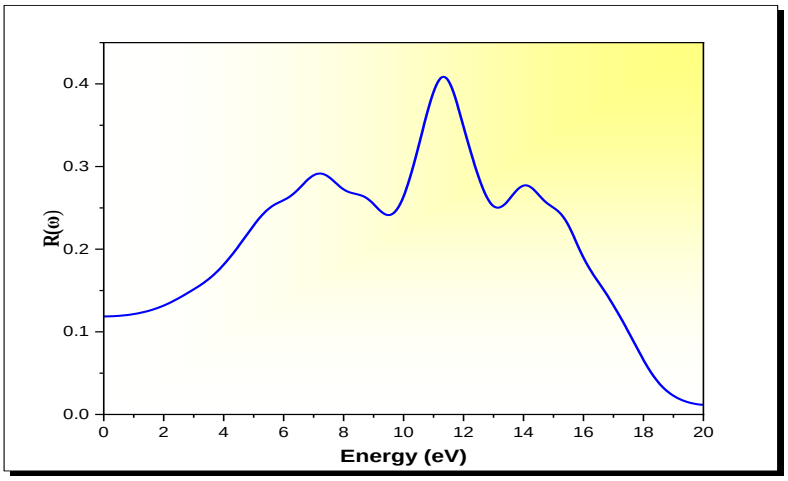

Figure 7. Reflectivity of $SrMg_2FeH_8$.

Figures 8 present the real and imaginary parts of the conductivity, which describe the material's interaction with electromagnetic radiation. The real and imaginary parts of the optical conductivity were calculated from the frequency-dependent complex dielectric function $\varepsilon(\omega)= \varepsilon_1(\omega) + i\varepsilon_2(\omega)$), using the following relations[47]:

$$\sigma_1(\omega) = \frac{\omega\varepsilon_2(\omega)}{4\pi} \quad , \quad \sigma_2(\omega) = \frac{\omega[1-\varepsilon_1(\omega)]}{4\pi} \tag{10}$$

These equations provide a direct connection between the dielectric response and the material's ability to conduct charge carriers under electromagnetic excitation, thereby offering valuable insight into its optoelectronic performance. The real part (figure 8.a) represents the dissipative component, which corresponds to the energy absorbed by the material and transformed into other forms, such as heat. It begins at 2.18 eV and exhibits a prominent peak with a maximum value of 5.36 at 6.97 eV, highlighting significant optical absorption due to electronic transitions in this energy range. This behavior indicates the contribution of interband transitions to the conductivity, particularly involving electronic states close to the Fermi level. The imaginary part (figure8.b), reflects the reactive component of the conductivity, which is associated with polarization effects and the energy temporarily stored in the system. It starts at zero energy, demonstrating that there is no reactive response at very low frequencies, and decreases to a minimum value of -3.60 at 5.15 eV. The negative values in the region illustrates the dominance of inductive forms of effects and indicate that the material is opposing the electric field at these energies. Beyond this value the imaginary conductivity is increasingly behaving suggesting a more complex interaction between polarization and electronic transitions at higher energy ranges.

This extensive analysis of the real and imaginary parts of the conductivity yields valuable information about the optoelectronic properties of the material. The separate peak of the real part and the distinct behaviors of the and imaginary parts of the conductivity in the low and high energy regions of the material consistently supports the prospect of using the material in optoelectronic devices, energy conversion, and other applications needing effective interaction with electromagnetic radiation.

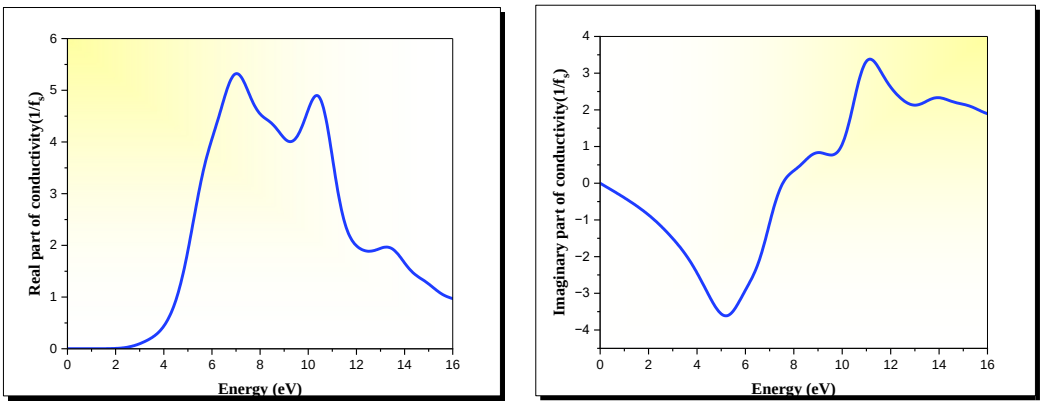

(a) (b)

Figure 8. a) Real part of conductivity, b) imaginary part for $SrMg_2FeH_8$.

3.3 Photocatalytic Properties

The process of photon absorption is key in determining the photocatalytic capability of added materials, especially semiconductors, whose functionality is dictated by band energy theory[48,49]. As an example, the photocatalytic material $SrMg_2FeH_8$ can absorb photon energy when illuminated with light with its wavelength equal to or greater than its bandgap energy

(E_g). This photon absorption results in electronic transitions from the valence band (VB) to the conduction band (CB) leading to the formation of electron-hole pairs (e^-/h^+). Then, under suitable light irradiation, the photogenerated charge carriers migrate to the surface of the photocatalyst and undergo oxidation and reduction reactions[49,50].

Electrons in the conduction band of the photocatalyst surface undergo reduction reactions, such as forming molecular hydrogen (H_2) with electron-acceptors, namely, H+ ions. Whereas holes in the valence band proceed in oxidation reactions to form highly reactive hydroxyl (OH) radicals and promote the degradation of organic pollutants to form simple products, like CO_2 and H_2O. Photocatalytic efficiency is directly related to the ability of the material to inhibit electron-hole recombination, as excess dissipation of recombination energy will dissipate absorbed energy through heat or light, thus limiting the overall efficiency of the process. To enable good photocatalytic performance $SrMg_2FeH_8$ must show high charge carrier mobility, long excited state lifetimes, and appropriate energy band alignment that is compatible with the redox potentials of target reactions. In this way, you can separate charge and migrate it to maximize the redox activity of your system for hydrogen evolution and organic pollutant degradation applications. Therefore, the photocatalytic mechanism of $SrMg_2FeH_8$ uses a combination of good phase light absorbed, charge separation, and surface redox reactions which implies that $SrMg_2FeH_8$ maintains promise as a viable material for advanced photocatalytic applications. The photocatalytic mechanism can be described by the following sequential redox reactions[51]:

$$(SrMg_2FeH_8) \xrightarrow{h\nu} h^+ + e^- \quad (11)$$

$$h^+ + H_2O \rightarrow OH + H^+ \quad (12)$$

$$e^- + O_2 \rightarrow O_2^- \quad (13)$$

$$O_2^- + H^+ \rightarrow HOO \quad (14)$$

$$e^- + HOO + H^+ \rightarrow H_2O_2 \quad (15)$$

$$H_2O_2 + e^- \rightarrow OH + OH^- \quad (16)$$

$$OH + organic\ pollutants \rightarrow intermediates \rightarrow degradation\ products \quad (17)$$

The redox potential and the energetic alignment of the band edges of adsorbed molecules are crucial, as they will regulate the migration dynamics and the separation efficiency of the photogenerated electron—hole pairs, and essentially drive the photocatalytic efficiency of a material. For $SrMg_2FeH_8$ to achieve high photocatalytic performance under visible light, it must satisfy three essential criteria: a sufficiently narrow bandgap to enable strong absorption in the visible spectrum, effective separation of charge carriers to limit recombination, and appropriate alignment of the valence and conduction band edges to drive the necessary redox reactions. The redox behavior of $SrMg_2FeH_8$ has been assessed through analysis of its conduction and valence band edge positions. These energy levels are estimated based on Mulliken's electronegativity approach in conjunction with the calculated bandgap of the

material. A positive VBM potential implies a strong oxidative capability of photogenerated holes, whereas a negative CBM potential indicates that the corresponding electrons exhibit strong reducing power. The positions of the VBM and CBM in $SrMg_2FeH_8$ can be determined using the following equations, derived from its electronegativity and bandgap values[51,52]:

$$E_{VB} = \boldsymbol{\chi} - E_e + \frac{1}{2}E_g \tag{18}$$

$$E_{CB} = E_{VB} - E_g \tag{19}$$

The edge potentials of the valence band (EVB) and conduction band (ECB) indicate the energetic locations of the valence and conduction bands. $\boldsymbol{\chi}$ designates the Mulliken electronegativity of the material being considered, calculated as the geometric mean of the $Mulliken$ electronegativities of its constituent compounds. During Mulliken's determination of the atom's electronegativity the electronegativity was determined from the arithmetic average of the electron affinity (the energy released when an electron is inserted into the neutral atom) and the first ionization energy (the energy needed to remove the weakliest bound electron from the atom). The reference energy standard is the hydrogen electrode scale, and therefore, the energy of free electrons is $E_e = 4.5\,eV$. E_g refers to the bandgap energy of $SrMg_2FeH_8$ calculated. The following table summarizes the key photocatalytic parameters obtained for $SrMg_2FeH_8$ [51,53].

Table 2. Photocatalytic parameters for SrMg2FeH8.

Material	$\boldsymbol{\chi}$ (eV)	E_g (eV)	E_{VB} (eV)	E_{CB} (eV)
$SrMg_2FeH_8$	5.99	2.251	2.61	0.36

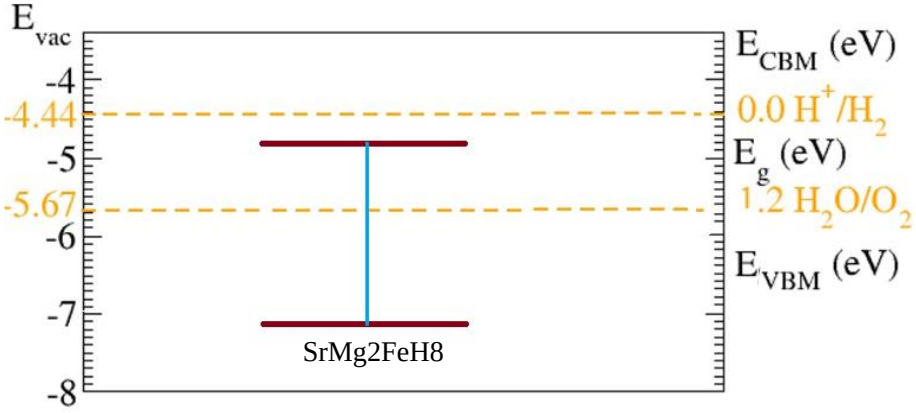

Figure 9: Photocatalytic diagram of SrMg2FeH8.

Figure 9 presents the photocatalytic properties of S $SrMg_2FeH_8$, characterized by a moderate energy gap (E_g = 2.251 eV), enabling efficient absorption within the visible light spectrum. Its valence band edge (E_{VB} = 2.61 eV) is well-positioned for oxidative reactions, particularly water oxidation, as it exceeds the required potential of +1.23 V versus the normal hydrogen electrode (NHE). However, the conduction band edge (E_{CB} = 0.36 eV) is slightly more negative than the reduction potential of H+ ions (0 V vs. NHE). While this value is thermodynamically sufficient

for hydrogen evolution, the limited driving force may slow the reaction kinetics and increase the likelihood of charge recombination. These limitations may negatively affect H+ reduction efficiencies and in turn, rates of hydrogen production; but additional catalysts, like noble metals or molecular catalysts, could mitigate these issues, promote electron transfer efficiencies, and a variety of photocatalytic performance. Therefore, while the $SrMg_2FeH_8$ material shows the opportunity to facilitate visible-light-driven photocataysis, the hydrogen production efficiencies would need further optimization through structural or compositional alterations.

4. CONCLUSION

This work represents a comprehensive evaluation of the optoelectronic and photocatalytic properties of $SrMg_2FeH_8$, demonstrating that it is a potentially interesting and versatile material for energy and environmental applications. The material's band gap of 2.251 eV results in the ability to absorb well in the visible light range and improve further on its photocatalytic and optoelectronic properties. The density of states (DOS) analysis showed that the electronic structure is significantly dependent on the interactions of Sr, Mg, Fe, and H orbitals, while the Fe d-orbitals were significant near the Fermi level. The optical properties such as refractive index, extinction coefficient, absorption spectrum, and energy loss function provided further evidence of strong interactions with light, particularly in the visible and ultraviolet regions. This is a potential indicator for the use of this material in applications such as photodetection, solar energy conversion, or photocatalytic processes. Photocatalytic assessments indicated that while the valance band edge is favorable to oxidative mechanisms such as water oxidation, the conduction band edge is only thermodynamically favorable for hydrogen evolution without limiting the kinetics of the reactions products by reducing the reaction energy value carried by the charge carriers in the photocatalytic reaction itself. The work highlighted the materials ability, yet futures work like the addition of co-catalysts or perhaps being able to take advantages of the materials inherent structure, could meaningfully enhance the materials capacity for hydrogen generation in this fashion.

ABBREVIATIONS

The following abbreviations are used in this manuscript:

DOS	Density of States
m-GGA	Modified Generalized Gradient Approximation
DFT	Density Functional Theory
VBM	Valence Band Maximum
CBM	Conduction Band Minimum
PDOS	Partial Density of States
Eg	Band Gap (Energy Gap)
VB	Valence Band
CB	Conduction Band
NHE	Normal Hydrogen Electrode

Author Contributions: HE and MK Conceptualization. HE and AE Methodology. HE, AE, and MK Software. OB and YL Validation. HE Formal analysis and investigation. HE and MK Resources. HE Data curation. HE Writing – original draft. AE Writing – review and editing. OB Visualization. YL Supervision. All authors read and approved the final manuscript.

Funding source: This research received no external funding

Data Availability Statement: This article has no associated data generated

Conflicts of Interest: The authors declare that the research was conducted in the absence of any commercial or financial relationships that could be construed as a potential conflict of interest.

AI- Declaration: The authors declare that no generative AI or AI-assisted technologies were used in the writing, analysis, or preparation of this manuscript. The entire work was carried out by the authors.

REFERENCES

[1] *L. George, S.K. Saxena, Structural stability of metal hydrides, alanates and borohydrides of alkali and alkali- earth elements: A review, Int. J. Hydrogen Energy 35 (2010) 5454–5470. https://doi.org/10.1016/j.ijhydene.2010.03.078.*

[2] *J. Bergsma, B.O. Loopstra, The crystal structure of calcium hydride, Acta Crystallogr. 15 (1962) 92–93. https://doi.org/10.1107/S0365110X62000225.*

[3] *M.K. Shahzad, S. Hussain, M.N. Khan, M.J. Aslam, R.M. Mohammed, V. Tirth, H. Alqahtani, A. Algahtani, T. Al-Mughanam, W. Azeem, Computational insights of double perovskite Na2CaCdH6 hydride alloy for hydrogen storage applications: a DFT investigation, Sci. Rep. 14 (2024) 25102. https://doi.org/10.1038/s41598-024-76062-0.*

[4] *H. Wu, W. Zhou, T.J. Udovic, J.J. Rush, T. Yildirim, Structure and vibrational spectra of calcium hydride and deuteride, J. Alloys Compd. 436 (2007) 51–55. https://doi.org/10.1016/j.jallcom.2006.07.042.*

[5] *A. Ejjabli, M. Karouchi, H. Errahoui, A. Laassouli, A. El haji, Y. Lachtioui, O. Bajjou, Comparative DFT Study of K2AgSbBr6 and K2NaScBr6: Exploring the Role of B'B" Cation Substitution on Material Properties, Atoms 13 (2025) 53. https://doi.org/10.3390/atoms13060053.*

[6] *A.F. Andresen, A.J. Maeland, D. Slotfeldt-Ellingsen, Calcium hydride and deuteride studied by neutron diffraction and NMR, J. Solid State Chem. 20 (1977) 93–101. https://doi.org/10.1016/0022-4596(77)90055-X.*

[7] *H. Smithson, C.A. Marianetti, D. Morgan, A. Van der Ven, A. Predith, G. Ceder, First-principles study of the stability and electronic structure of metal hydrides, Phys. Rev. B 66 (2002) 144107. https://doi.org/10.1103/PhysRevB.66.144107.*

[8] *N.E. Brese, M. O'Keeffe, R.B. Von Dreele, Synthesis and crystal structure of SrD2 and SrND and bond valence parameters for hydrides, J. Solid State Chem. 88 (1990) 571–576. https://doi.org/10.1016/0022-4596(90)90255-V.*

[9] *H. Errahoui, M. Karouchi, A. Ejjabli, A. El haji, A. Laassouli, O. Ait El Alia, S. Chaji, Y. Lachtioui, O. Bajjou, Impact of Calcium Doping on the Electronic and Optical Characteristics of Strontium Hydride (SrH2): A DFT Study, Atoms 12 (2024) 55. https://doi.org/10.3390/atoms12110055.*

[10] *A.G. Akerdi, S.H. Bahrami, Application of heterogeneous nano-semiconductors for photocatalytic advanced oxidation of organic compounds: A review, J. Environ. Chem. Eng. 7 (2019). https://doi.org/10.1016/j.jece.2019.103283.*

[11] H.W. Langmi, G.S. McGrady, R. Newhouse, E. Rönnebro, Mg2FeH6–LiBH4 and Mg2FeH6–LiNH2 composite materials for hydrogen storage, Int. J. Hydrogen Energy 37 (2012) 6694–6699. https://doi.org/10.1016/j.ijhydene.2012.01.020.

[12] T.D. Humphries, D.A. Sheppard, C.E. Buckley, Recent advances in the 18-electron complex transition metal hydrides of Ni, Fe, Co and Ru, Coord. Chem. Rev. 342 (2017) 19–33. https://doi.org/10.1016/j.ccr.2017.04.001.

[13] A. Ejjabli, M. Karouchi, H. Errahoui, O. Bajjou, J. Guerroum, A. Elhajji, K. Rahmani, Y. Lachtioui, Electronic and Optical Properties of Double Perovskite Oxide $LaFeWO_6$: A Theoretical Understanding from DFT Calculations, E3S Web of Conferences 582 (2024) 02001. https://doi.org/10.1051/e3sconf/202458202001.

[14] E.M. Dematteis, M.B. Amdisen, T. Autrey, J. Barale, M.E. Bowden, C.E. Buckley, Y.W. Cho, S. Deledda, M. Dornheim, P. de Jongh, J.B. Grinderslev, G. Gizer, V. Gulino, B.C. Hauback, M. Heere, T.W. Heo, T.D. Humphries, T.R. Jensen, S.Y. Kang, Y.-S. Lee, H.-W. Li, S. Li, K.T. Møller, P. Ngene, S. Orimo, M. Paskevicius, M. Polanski, S. Takagi, L. Wan, B.C. Wood, M. Hirscher, M. Baricco, Hydrogen storage in complex hydrides: past activities and new trends, Progress in Energy 4 (2022) 032009. https://doi.org/10.1088/2516-1083/ac7499.

[15] M. Hirscher, V.A. Yartys, M. Baricco, J. Bellosta von Colbe, D. Blanchard, R.C. Bowman, D.P. Broom, C.E. Buckley, F. Chang, P. Chen, Y.W. Cho, J.-C. Crivello, F. Cuevas, W.I.F. David, P.E. de Jongh, R. V. Denys, M. Dornheim, M. Felderhoff, Y. Filinchuk, G.E. Froudakis, D.M. Grant, E.MacA. Gray, B.C. Hauback, T. He, T.D. Humphries, T.R. Jensen, S. Kim, Y. Kojima, M. Latroche, H.-W. Li, M. V. Lototskyy, J.W. Makepeace, K.T. Møller, L. Naheed, P. Ngene, D. Noréus, M.M. Nygård, S. Orimo, M. Paskevicius, L. Pasquini, D.B. Ravnsbæk, M. Veronica Sofianos, T.J. Udovic, T. Vegge, G.S. Walker, C.J. Webb, C. Weidenthaler, C. Zlotea, Materials for hydrogen-based energy storage – past, recent progress and future outlook, J. Alloys Compd. 827 (2020) 153548. https://doi.org/10.1016/j.jallcom.2019.153548.

[16] B. Huang, K. Yvon, P. Fischer, Strontium dimagnesium iron octahydride, SrMg2FeH8, containing octahedral [FeH6]4- complex anions, J. Alloys Compd. 187 (1992) 227–232. https://doi.org/10.1016/0925-8388(92)90536-I.

[17] H. Errahoui, M. Karouchi, A. Bakour, A. Ejjabli, A. El Haji, A. Laassouli, Y. Lachtioui, O. Bajjou, Tailoring the optoelectronic and photocatalytic properties of MgH2 through Sr and Ca doping for sustainable energy technologies, Chemical Papers (2026). https://doi.org/10.1007/s11696-026-04727-3.

[18] Y. Goto, T. Hisatomi, Q. Wang, T. Higashi, K. Ishikiriyama, T. Maeda, Y. Sakata, S. Okunaka, H. Tokudome, M. Katayama, S. Akiyama, H. Nishiyama, Y. Inoue, T. Takewaki, T. Setoyama, T. Minegishi, T. Takata, T. Yamada, K. Domen, A Particulate Photocatalyst Water-Splitting Panel for Large-Scale Solar Hydrogen Generation, Joule 2 (2018) 509–520. https://doi.org/10.1016/j.joule.2017.12.009.

[19] H.M.N. Ullah, M. Rizwan, S.S. Ali, Z. Usman, C. Cao, A DFT study of optical, elastic, mechanical, and overall water-splitting photocatalytic properties of pristine and Cd substituted BaZrO3: A lead free environment friendly material, Materials Science and Engineering: B 286 (2022) 116041. https://doi.org/10.1016/j.mseb.2022.116041.

[20] A. Laassouli, M. Karouchi, A. Ejjabli, A. El Haji, H. Errahoui, K. Rahmani, Y. Lachtioui, O. Bajjou, Halide-driven tuning of structural, electronic, and optical properties in lead-free K2AgSbX6 (X = I, Br, Cl) double perovskites: a DFT study, J. Mol. Model. 32 (2026) 94. https://doi.org/10.1007/s00894-026-06669-9.

[21] S.J. Clark, M.D. Segall, C.J. Pickard, P.J. Hasnip, M.I.J. Probert, K. Refson, M.C. Payne, First principles methods using CASTEP, Z. Kristallogr. Cryst. Mater. 220 (2005) 567–570. https://doi.org/10.1524/zkri.220.5.567.65075.

[22] M.D. Segall, P.J.D. Lindan, M.J. Probert, C.J. Pickard, P.J. Hasnip, S.J. Clark, M.C. Payne, First-principles simulation: ideas, illustrations and the CASTEP code, Journal of Physics: Condensed Matter 14 (2002) 2717–2744. https://doi.org/10.1088/0953-8984/14/11/301.

[23] P.J. Hasnip, K. Refson, M.I.J. Probert, J.R. Yates, S.J. Clark, C.J. Pickard, Density functional theory in the solid state, Philosophical Transactions of the Royal Society A: Mathematical, Physical and Engineering Sciences 372 (2014) 20130270. https://doi.org/10.1098/rsta.2013.0270.

[24] J.P. Perdew, K. Burke, M. Ernzerhof, Generalized Gradient Approximation Made Simple, Phys. Rev. Lett. 77 (1996) 3865–3868. https://doi.org/10.1103/PhysRevLett.77.3865.

[25] J.M. Del Campo, J.L. Gázquez, S.B. Trickey, A. Vela, Non-empirical improvement of PBE and its hybrid PBE0 for general description of molecular properties, Journal of Chemical Physics 136 (2012). https://doi.org/10.1063/1.3691197.

[26] G.S. Painter, Improved correlation corrections to the local-spin-density approximation, Phys. Rev. B 24 (1981) 4264–4270. https://doi.org/10.1103/PhysRevB.24.4264.

[27] H.J. Monkhorst, J.D. Pack, Special points for Brillouin-zone integrations, Phys. Rev. B 13 (1976) 5188–5192. https://doi.org/10.1103/PhysRevB.13.5188.

[28] A. Ejjabli, M. Karouchi, M. Al-Hattab, O. Bajjou, K. Rahmani, Y. Lachtioui, Investigation of lead-free halide K2AgSbBr6 double Perovskite's structural, electronic, and optical properties using DFT functionals, Chemical Physics Impact 9 (2024) 100656. https://doi.org/10.1016/j.chphi.2024.100656.

[29] M. KAROUCHI, A. EJJABLI, S. SAMINE, O. BAJJOU, Y. LACHTIOUI, Enhancing the Optoelectronic Properties of TiPbO3 perovskite through Lanthanum Doping, Solar Energy and Sustainable Development Journal (2024) 142–155. https://doi.org/10.51646/jsesd.v14iSI_MSMS2E.397.

[30] A. EL Haji, M. Karouchi, A. Ejjabli, H. Errahoui, A. Laassouli, M. Harb, Y. Lachtioui, O. Bajjou, First-principles investigation of structural, mechanical, electronic, optical, and thermodynamic properties of perovskite hydrides XRuH3 (X=Mg, Ca, Sr, Ba) for hydrogen storage, Int. J. Hydrogen Energy 223 (2026) 154379. https://doi.org/10.1016/j.ijhydene.2026.154379.

[31] Y. Goto, T. Hisatomi, Q. Wang, T. Higashi, K. Ishikiriyama, T. Maeda, Y. Sakata, S. Okunaka, H. Tokudome, M. Katayama, S. Akiyama, H. Nishiyama, Y. Inoue, T. Takewaki, T. Setoyama, T. Minegishi, T. Takata, T. Yamada, K. Domen, A Particulate Photocatalyst Water-Splitting Panel for Large-Scale Solar Hydrogen Generation, Joule 2 (2018) 509–520. https://doi.org/10.1016/j.joule.2017.12.009.

[32] K. Takanabe, Photocatalytic Water Splitting: Quantitative Approaches toward Photocatalyst by Design, ACS Catal. 7 (2017) 8006–8022. https://doi.org/10.1021/acscatal.7b02662.

[33] I.H. Chowdhury, S. Kundu, M.K. Naskar, Template-free hydrothermal synthesis of MgO-TiO2 microcubes toward high potential removal of toxic water pollutants, Journal of Physics and Chemistry of Solids 112 (2018) 171–178. https://doi.org/10.1016/j.jpcs.2017.09.021.

[34] A. Laassouli, M. Karouchi, A. Ejjabli, Y. Lachtioui, O. Bajjou, DFT study on K2AgSbI6: Exploring the electronic, optical, and elastic properties of a double

perovskite, Solid State Commun. 402 (2025) 115947. https://doi.org/10.1016/j.ssc.2025.115947.

[35] H. Benmhidi, H. Rached, D. Rached, M. Benkabou, Ab Initio Study of Electronic Structure, Elastic and Transport Properties of Fluoroperovskite LiBeF3, J. Electron. Mater. 46 (2017) 2205–2210. https://doi.org/10.1007/s11664-016-5159-0.

[36] A. Ayyaz, G. Murtaza, Y. Bakkour, M. mana Al-Anazy, Impact of Halide Ion Occupancy on Thermodynamic, Mechanical, Electro-optic, and Electron Transport Characteristics of Rb2CuAsX6 (X = F, Cl, Br) Double Perovskites Using Density Functional Theory, J. Inorg. Organomet. Polym. Mater. (2024). https://doi.org/10.1007/s10904-024-03079-3.

[37] A. Laassouli, L. Moulaoui, A. Najim, H. Errahoui, K. Rahmani, Y. Lachtioui, O.B. Omar Bajjou, Phosphorus Doping Effects on the Optoelectronic Properties of $K_2AgAsBr_6$ Double Perovskites for Photovoltaic Applications, Solar Energy and Sustainable Development Journal (2024) 1–11. https://doi.org/10.51646/jsesd.v14iSI_MSMS2E.407.

[38] H. errahoui, M. karouchi, A. Ejjabli, A. Laassouli, A. El Haji, Y. Lachtioui, O. Bajjou, DFT-based investigation of Ca_2H_3Br and Ba_2H_3I: electronic, optical, and hydrogen storage properties for energy applications, Phys. Scr. (2025). https://doi.org/10.1088/1402-4896/ae2992.

[39] M. Karouchi, A. Ejjabli, O. Bajjou, J. Guerroum, M. Al-Hattab, M.A. Basyooni-M. Kabatas, K. Rahmani, Y. Lachtioui, Investigating the structural, electronic, and optical properties of the novel double perovskite K2AgBiI6 using DFT, Front. Mater. 11 (2024). https://doi.org/10.3389/fmats.2024.1448400.

[40] A. Laassouli, M. Karouchi, A. Ejjabli, A. El Haji, H. Errahoui, Y. Lachtioui, O. Bajjou, Novel Insights into the Electric Field-Driven Electronic and Optical Behavior of K2AgSbI6 via DFT, J. Electron. Mater. (2026). https://doi.org/10.1007/s11664-025-12643-7.

[41] H. Errahoui, M. Karouchi, A. Ejjabli, A. Laassouli, A. EL Haji, Y. Lachtioui, O. Bajjou, Hydrogen Storage and Energy Applications of H6X2N3Na (X = K; Rb): AIMD and First-Principles Study Approach, J. Electron. Mater. (2026). https://doi.org/10.1007/s11664-026-12736-x.

[42] A. Laassouli, M. Karouchi, A. Ejjabli, H. Errahoui, A. El Haji, Y. Lachtioui, O. Bajjou, Structural, mechanical, electronic, and optoelectronic properties of wide-band-gap hydride perovskite BaNaH3Pt from hybrid density functional theory, Next Materials 11 (2026) 101803. https://doi.org/10.1016/j.nxmate.2026.101803.

[43] A. Laassouli, M. Karouchi, A. Ejjabli, H. Errahoui, A. El Haji, Y. Lachtioui, O. Bajjou, Tuning optoelectronic properties in BaNaH3X (X = Ni, Pd, Pt) perovskite hydrides: a DFT-based analysis, J. Mol. Model. 32 (2026) 39. https://doi.org/10.1007/s00894-025-06624-0.

[44] H. Errahoui, M. Karouchi, A. Ejjabli, A. Elhaji, K. Rahmani, M. Harb, Y. Lachtioui, O. Bajjou, DFT study of optoelectronic properties in pristine and Ba-doped SrH2 for enhanced energy storage and photonic applications, Journal of Materials Science: Materials in Engineering (2026). https://doi.org/10.1186/s40712-026-00405-0.

[45] K.W. Guji, T.A. Geleta, N. Bouri, V.J. Ramirez Rivera, First principles study on the structural stability, mechanical stability and optoelectronic properties of alkali-based single halide perovskite compounds XMgI3 (X = Li/Na): DFT insight, Nanoscale Adv. 6 (2024) 4479–4491. https://doi.org/10.1039/d4na00305e.

[46] S. Ahmed, W. Zulfiqar, F. Javed, H. Arshad, G. Abbas, A. Laref, S.M. Alay-e-Abbas, Accurate first-principles evaluation of structural, electronic, optical and photocatalytic

properties of BaHfO3 and SrHfO3 perovskites, J. Alloys Compd. 892 (2022) 162071. https://doi.org/10.1016/j.jallcom.2021.162071.

[47] A. Ejjabli, M. Karouchi, H. Errahoui, A. El Haji, Y. Lachtioui, O. Bajjou, First-principles comparative analysis of the physical properties of K2AgMBr6 (M = Sb, Bi, P, In) perovskites: Promising candidates for clean energy applications, Next Materials 9 (2025) 101321. https://doi.org/10.1016/j.nxmate.2025.101321.

[48] M. Rochkind, S. Pasternak, Y. Paz, Using dyes for evaluating photocatalytic properties: A critical review, Molecules 20 (2015) 88–110. https://doi.org/10.3390/molecules20010088.

[49] H. Errahoui, M. Karouchi, A. Ejjabli, A. Laassouli, A. El haji, Y. Lachtioui, O. Bajjou, Photocatalytic Properties of XH2 (X = Ca, Ba, Mg, and Sr): Unlocking Potential for Sustainable Energy and Environmental Applications, Catal. Letters 155 (2025) 359. https://doi.org/10.1007/s10562-025-05193-4.

[50] L. Sajid, M.U. Saeed, S.H. Mashadi, S.S. Abid, S. Pervaiz, Z. Ali, Y.M. Alanazi, A.U.R. Bacha, Y. Saeed, Ab initio study of electronic, elastic, thermodynamic, photocatalytic properties of double antiperovskite, Cs6AgBiX2 (X = Cl, Br, I), RSC Adv. 14 (2024) 35348–35359. https://doi.org/10.1039/d4ra05661b.

[51] A. Mera, M.A. Rehman, Z. ur Rehman, U. Farrukh, M. Usman, A. Rehman, Computational exploration of oxide-based double perovskites Sr2MgWO6 and Ba2BiVO6 for photocatalysts for sustainable degradation processes, Inorg. Chem. Commun. 162 (2024). https://doi.org/10.1016/j.inoche.2024.112259.

[52] M. Karouchi, Y. Lachtioui, O. Bajjou, Transformation of BaTiO3 electro-optical properties through graphene oxide integration for high-performance photovoltaic applications, Mater. Sci. Energy Technol. (2025). https://doi.org/10.1016/j.mset.2025.07.003.

[53] D. Hong, W. Zeng, B. Tang, M. Zhong, Q.-J. Liu, Density functional theory study on the electronic and photocatalytic properties of different phases for Ba2BiTaO6, J. Solid State Chem. 293 (2021) 121790. https://doi.org/10.1016/j.jssc.2020.121790.